Available online at www.sciencedirect.com
ScienceDirect
Journal of Volcanology and Geothermal Research 156 (2006) 302–314
Journal of volcanology and geothermal research
www.elsevier.com/locate/jvolgeores

Spectroscopic FTIR imaging of water species in silicic volcanic glasses and melt inclusions: An example from the Izu-Bonin arc

Richard Wysoczanski *, Kenichiro Tani

Institute for Research on Earth Evolution, Japan Agency for Marine–Earth Science and Technology, 2–15 Natsushima-cho, Yokosuka, Kanagawa 237-0061, Japan

Received 8 April 2005; accepted 2 March 2006
Available online 9 May 2006

Abstract

Recent advances in FTIR spectroscopic imaging allow images of elements or molecules such as water to be constructed on samples over a large (sub mm) area. The imaging detector consists of 64×64 channels providing 4096 individual spectra simultaneously collected over a spectral range of 4000–900 cm^{-1}. The wavelength range includes measurable peaks for water and carbon species, making it ideal for the analysis of volcanic glasses, particularly melt inclusions. Advantages of spectroscopic imaging include high spatial resolution (~ 5 μm), allowing the analysis of melt inclusions too small to be analysed by other micro-FTIR techniques, and the acquisition of high definition in situ images of the materials analysed. The technique is applied to the analysis of water species concentrations and distribution in silicic volcanic glasses from Sumisu Caldera and Torishima Volcano in the Izu-Bonin arc to test the application of imaging to geologic samples. Results obtained are found to be comparable to analyses by conventional micro-FTIR techniques, with similar precision, but greater spatial resolution. Groundmass glasses from Sumisu Caldera dacites contain 1.2–1.4 wt.% H_2O and an obsidian sample from Torishima Volcano contains 0.2 wt.% H_2O, consistent with water saturation at their respective pressures of eruption. Melt inclusions in honeycomb plagioclase from Sumisu Caldera have higher water contents (1.02–1.38 wt.% H_2O) than inclusions from Torishima Volcano plagioclase (0.22–0.41 wt.% H_2O). Despite evidence for many inclusions being trapped wholly within honeycomb plagioclase, low water contents similar to those of the groundmass glasses suggest that the inclusions underwent water loss by degassing and/or diffusion. Alternatively, if low water contents of the melt inclusions reflect the composition of the magma at the time of entrapment, then the magma can be constrained as having originated from a water-poor source. Despite the ambiguity in initial water contents of the magma, the anhydrous mineral assemblage of all Sumisu Caldera and Torishima silicic rocks indicates an origin from a water-poor source, consistent with models for partial melting of water-poor mafic lower-mid crust, rather than melting of wet lower-mid crust or differentiation from basaltic magmas.
© 2006 Elsevier B.V. All rights reserved.

Keywords: FTIR spectroscopic imaging; Izu–Bonin arc; crustal growth; glass water contents; honeycomb plagioclase; melt inclusions

1. Introduction

Fourier Transform Infra-Red (FTIR) absorption spectroscopy is an analytical technique based on the frequency at which chemical bonds vibrate when subjected to electromagnetic radiation passed through (transmission mode), or reflected off (reflection mode), a subject of interest. As functional groups and polar bonds of elements (e.g. Si, O, H, C and N) absorb radiation at specific wavelengths, FTIR spectroscopy can be used to both qualitatively and quantitatively measure these elements. FTIR analyses of geologic materials, particu-

* Corresponding author. Tel.: +81 468 67 9631; fax: +81 468 67 9625.
E-mail address: richardw@jamstec.go.jp (R. Wysoczanski).

0377-0273/$ - see front matter © 2006 Elsevier B.V. All rights reserved.
doi:10.1016/j.jvolgeores.2006.03.024

larly natural and experimental glasses, minerals and melt inclusions, have been undertaken for many years (see Ihinger et al., 1994 for a review). An essential area of research is the analysis of water in volcanic glasses from subduction zones, spreading ridges and hotspots, to examine its critical role in magmatic processes and mechanisms of crustal growth, such as melting, crystallization and assimilation (e.g. recent studies of Sobolov and Chaussidon, 1996; Danyushevsky et al., 2000; Newman et al., 2000; Dixon and Clauge, 2001; Luhr, 2001; Dixon et al., 2002; Nichols et al., 2002; Wysoczanski et al., 2006). These are transmission micro-

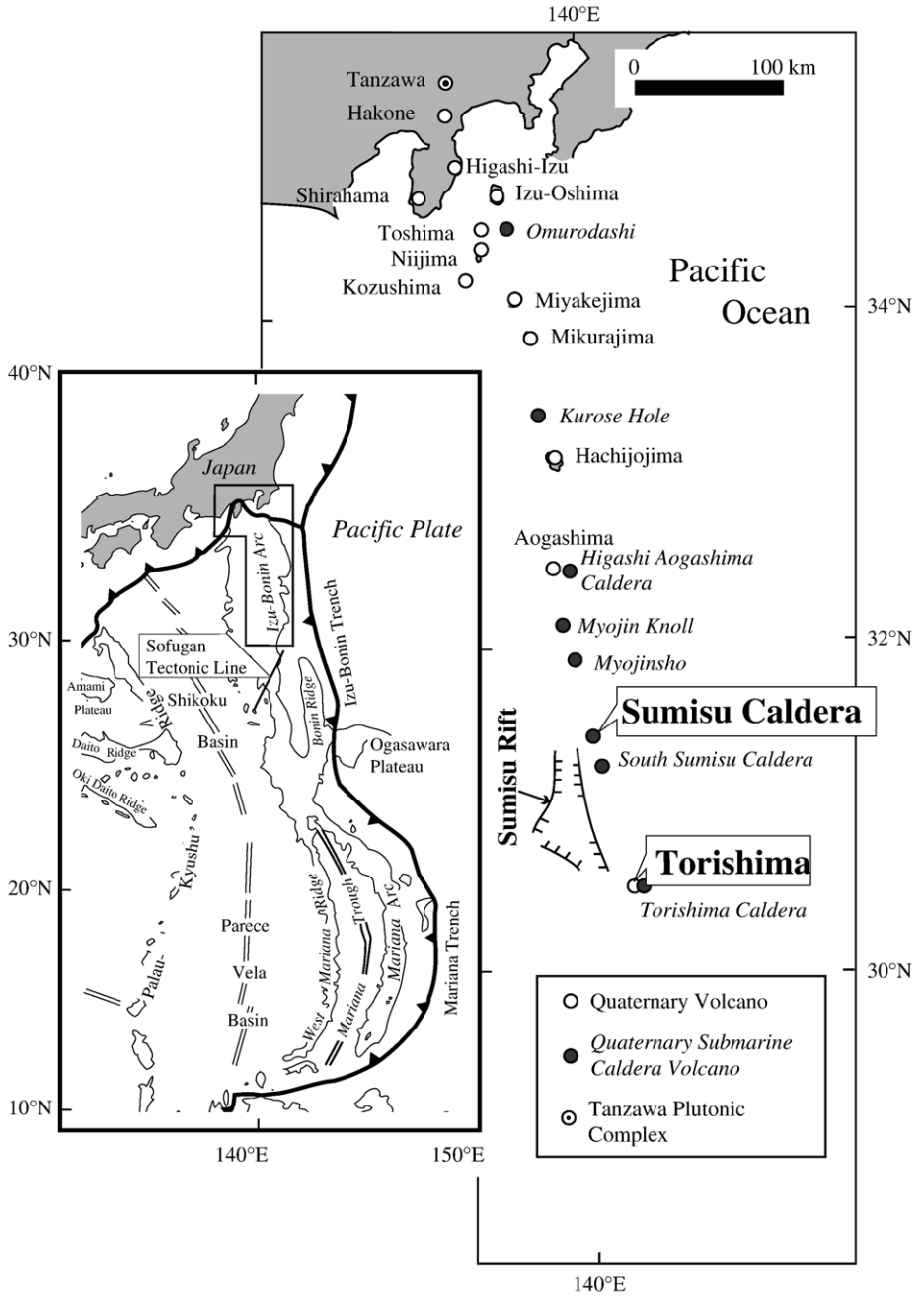

Fig. 1. Map of the Izu–Bonin arc showing Quaternary volcanoes and submarine calderas (from Tamura and Tatsumi, 2002). The location of the Tanzawa tonalite, discussed in the text, is also shown. The double lines identify spreading centres, now extinct in the Shikoku and Parece Vela basins, but active in the Mariana trough to the south of the Izu–Bonin arc.

FTIR studies that utilise an attached microscope to analyse small areas (typically <200 μm) of a sample. The result is a single high-resolution infra-red spectrum, providing an average water species content for the area analysed, with limited spatial resolution.

An important advance in FTIR spectroscopy in the past decade has been the advent of spectroscopic imaging (e.g. Lewis et al., 1995), a technique that allows a map of an element or molecule of interest to be constructed over a large (sub mm) area from multiple spectra collected by transmission or reflection mode. More recent developments by Varian Inc. allow optical maps of a band of interest to be constructed from 4096 simultaneously collected high-resolution spectra, with a spatial resolution of just 5 μm. As well as improved spatial resolution, the simultaneous collection of spectra distinguishes this technique from image maps, which are a composite of individual spectra collected sequentially to form a large composite image.

An increasing number of studies have utilised the spectroscopic imaging technique, however, with the exception of one study on cherts from Kanto Mountain, Japan (Ito and Nakashima, 2002), these studies have largely been restricted to the materials and biological sciences, and geologic materials have not been analysed. The objective of this study is to examine the application of spectroscopic imaging to volatile species analysis of volcanic materials. The technique and sample preparation are described, and silicic volcanic rocks from the Izu–Bonin volcanic arc are analysed for water species contents, and the data compared with analyses acquired using conventional micro-FTIR data spectroscopy. The relevance of the results to existing models of silicic magma genesis and crustal growth for the Izu–Bonin arc is then discussed.

2. Models for crustal growth in the Izu–Bonin arc and sample description

The Izu–Bonin arc, which lies between latitudes of 35°N and 30°N, contains a number of Quaternary island volcanoes and submarine silicic calderas (Nagaoka et al., 1991; Yuasa et al., 1991), such as Torishima Volcano and Sumisu Caldera in the central Izu–Bonin arc. The dominant composition of the Izu–Bonin arc was thought to be basaltic (Aramaki and Ui, 1978). Recent studies, however, have identified a number of rhyolitic submarine calderas (e.g. Fiske et al., 2001) and the arc is now considered bimodal in composition (Tamura and Tatsumi, 2002). Seismic transects have identified a middle crust (6 km/s P-wave velocity layer) up to 5 km thick (Takahashi et al., 1998), interpreted to be similar in composition to the Tanzawa tonalite pluton accreted on to Honshu arc (Kawate and Arima, 1998). Over the length of the Izu–Bonin arc, the composition of the middle crust may vary, and include more water-rich amphibolite, or dry, perhaps restitic, crust. (Fig. 1).

An origin for silicic magmas in this intra-oceanic arc system may be from fractionation of basaltic magmas (e.g. Vogel et al., 2004). More recently, partial melting of water-poor andesitic middle crust represented by the Tanzawa pluton (Tamura and Tatsumi, 2002; Shukuno et al., 2006-this issue), or water-rich amphibolitic lower crust (Nakajima and Arima, 1998) have been proposed as the source of Izu–Bonin silicic magmas. Determining the water content of silicic rocks may help distinguish between these models, as water content is dependent on the process of magma generation and source composition. Differentiation of basaltic magmas will result in water-rich silicic magmas. Partial melting of lower or middle crust will generate silicic magmas with water contents that reflect the composition of the protolith: high and low water contents for magmas sourced from amphibolite and dry andesitic crust, respectively.

Two dacites from Sumisu Caldera and a non-vesiculated obsidian from Torishima Volcano were selected for analysis of water contents to compare the imaging-FTIR technique to the conventional micro-FTIR method, and to provide important constraints on the genesis of silicic rocks in the Izu–Bonin arc. The Sumisu samples, 1391-R2 and 1394-R2A, were collected at water depths of 923 and 915 m, respectively, on separate dives by the manned submersible Shinkai 2000 as part the R/V *Natsushima* NT02-10 cruise. They consist of 90% groundmass and 10% phenocrysts (75% plagioclase, with minor amounts of clinopyroxene, orthopyroxene and opaque minerals). The Torishima Volcano sample (TS27-48) was collected from a subaerial tuff breccia. The sample consists of rhyolitic glass and has a phenocryst assemblage of plagioclase, olivine, clinopyroxene, orthopyroxene and titanomagnetite. Plagioclase from all samples occurs as clear euhedral plagioclase and as honeycomb plagioclase with resorbed and sieve textures. Importantly, the honeycomb plagioclases contain abundant melt inclusions in their interiors, providing direct samples of the magma, and therefore the magma water content, at the time they were entrapped.

3. Analytical techniques

3.1. Sample preparation

To prepare a sample for transmission FTIR spectroscopy, the sides of the sample must be parallel and both

polished to allow the IR beam to pass through the sample without scattering. A chip of each sample was cut as a thin section domino block and ground and polished using silicon carbide grit and 1 μm diamond paste to provide a flat highly polished surface. The sample was then adhered to a glass slide, polished side down, using crystal bond epoxy. The exposed surface was ground and polished as for the previous side, before removing the wafer from the glass slide by immersing it in acetone, which dissolves epoxy. Several further immersions in acetone were required to remove residual epoxy from the samples. The result was a thin (approximately 20–50 μm thick) freestanding doubly polished wafer free of any epoxy or binding agent, and suitable for micro-FTIR analysis. One concern with thin wafers, such as the 22–26 μm Torishima wafer, is their susceptibility to breakage. The thicker (40–50 μm) Sumisu sample wafers analysed here, however, were more manageable, with only minor splintering of the wafers into smaller pieces.

3.2. FTIR spectrometry

FTIR analyses were performed on a Varian FTS Stingray 7000 Micro Image Analyser spectrometer at the Institute for Research on Earth Evolution (IFREE). Infra-Red spectra, which consisted of 512 scans at a resolution of 4 cm^{-1}, were collected using a water-cooled ceramic source and a Ge-coated KBr beamsplitter. The beam path was continuously purged with N_2 gas to minimize the interference of atmospheric water on the measured spectra. The sample was placed on a water-free KBr base for support, and the background scan and sample analyses were taken through the KBr base under the same analytical conditions.

Conventional micro-FTIR analyses (hereafter termed 'micro-FTIR') using an attached UMA 600 microscope were obtained over a wavelength range of ν=7000–700 cm^{-1}, with a liquid-nitrogen cooled $HgCdTe_2$ (MCT) detector and an aperture set at 20 μm square. This provided a strong intensity and detector response for the mid-IR water absorbance bands.

Spectroscopic imaging ('imaging-FTIR') analyses were performed using an attached Varian Inc. Lancer Focal Plane Array (FPA) camera, which is an infrared photovoltaic MCT array detector consisting of 64×64 channels, providing 4096 individual spectra over the spectral range 4000–900 cm^{-1}. Each channel has a spatial resolution of 5 μm, resulting in a single 350×350 μm image. The FPA detector is highly sensitive with each channel equal to a single point MCT detector, as used with micro-FTIR analyses. Each 512-scan analysis took approximately 12 min to complete. With every analysis, some channels become saturated due to electronic difficulties. The number of these 'bad pixels' is typically 6–8; <0.2% of all channels. The noise level of IR spectra is approximately 0.2% transmission. However, this error can be higher for water absorption peaks due to

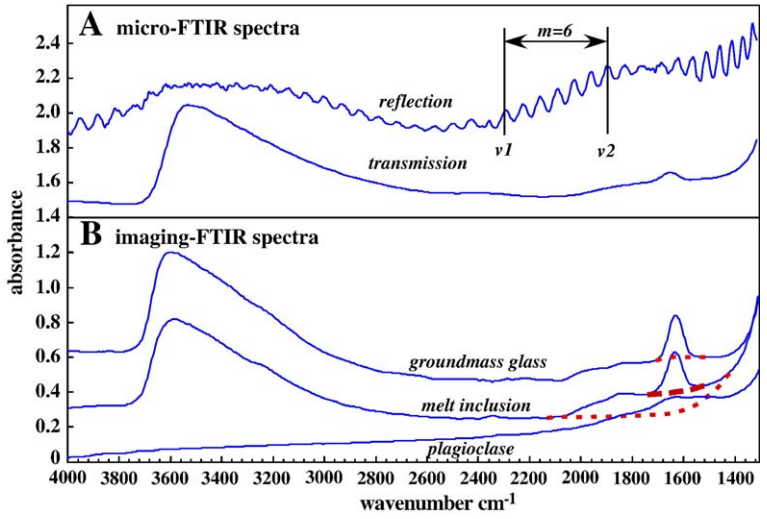

Fig. 2. Representative spectra of Sumisu Caldera glass and mineral phases. (A) Micro-FTIR spectra of groundmass glass acquired in both reflection and transmission mode. Reflection spectra are used to determine thickness of the sample from the spacing of interference patterns (see text). (B) Transmission spectra acquired from individual channels of spectroscopic images (spatial resolution of 5 μm). The position of the baseline for the 1630 cm^{-1} peak is difficult to determine, and can be selected as any of the dashed lines shown on this peak on melt inclusion and groundmass glass spectra. The baseline selected here, after King et al. (2002), is the thick dashed line shown on the melt inclusion spectra, intermediate to the other extremes. The uncertainty in this baseline position can impart a significant error on molecular water determinations.

interference from atmospheric water. The high efficiency of the gas purge system minimizes this error to a maximum of 0.5% of the peak height.

3.3. Determination of water species concentration

FTIR absorbance bands over the wavelength range measurable by the FPA camera (4000–900 cm^{-1}) include the fundamental OH stretching vibration ($\nu 1$) at 3550 cm^{-1}, and the fundamental HOH bending vibration ($\nu 2$) at 1630 cm^{-1} (Nakamoto, 1978; Ihinger et al., 1994). The concentration (c) of total dissolved water (H_2O_{tot}) and water dissolved as molecular water (H_2O_{mol}) can be determined from the absorbance bands at 3550 and 1630 cm^{-1}, respectively, by applying a modified Beer–Lambert law (Ihinger et al., 1994):

$$c = M\mathrm{Av}/\partial\rho\varepsilon$$

where M is the molar mass of the analyte (18.015 for H_2O), Av is the height or area of the spectral band of interest, ∂ and ρ are the thickness (cm) and density (g/l) of the sample, and ε is the molar absorptivity (l mol^{-1} cm) of the sample. The proportion of water occurring as OH in the glasses was taken as the difference between measured total water and molecular water contents.

Absorbance heights were determined using a flat, straight baseline for the 3350 cm^{-1} band, and a French curve for the 1630 cm^{-1} band (Fig. 2), following the method of King et al. (2002). Glass densities were calculated from chemical compositions (Shukuno et al., 2006-this issue; Tani unpublished data) based on the formulae of R. Lange, as discussed by Luhr (2001). The molar absorptivity for molecular water at ν=1630 cm^{-1} ($\varepsilon^{1\tilde{6}30}$ used here was $\varepsilon^{1\tilde{6}30}$=55±2 (Newman et al., 1986). For total water, a molecular absorptivity of $\varepsilon^{1\tilde{6}30}$=90±2 (Hauri et al., 2002) was used, which is similar to the 88±2 value of Dobson et al. (1989).

Sample thickness of the Sumisu samples were measured using a Mitutoyo micrometer, which has an estimated uncertainty of ±2–5 μm, (e.g. Agrinier and Jendrzejewski, 2000; Luhr, 2001; King et al., 2002). Melt inclusions not exposed on both sides of the wafer had their thickness estimated using a microscope reticule, and from estimation of the geometry of the inclusion (Signorelli et al., 1999). This method may impart significant error if the dimensions of the inclusions are not symmetrical. Thickness measurements for the thin TS27-48 wafer were measured from reflection spectra at each analytical point.

Table 1
Micro-FTIR analyses

Sample	Abs (3550 cm^{-1})	Abs (1630 cm^{-1})	Thickness (cm)	H_2O_{mol} wt.%	OH^- wt.%	H_2O_{tot} wt.%
1391-R2 groundmass						
1391-G1.1	0.56	0.25	0.0040	0.86	0.31	1.17
1391-G2.1	0.46	0.19	0.0034	0.76	0.38	1.14
1391-G3.1	0.46	0.21	0.0034	0.85	0.29	1.13
1391-G4.1	0.51	0.22	0.0036	0.85	0.35	1.20
1391-G5.1	0.48	0.22	0.0036	0.83	0.29	1.13
1391-G6.1	0.50	0.22	0.0036	0.82	0.34	1.17
1391-G7.1	0.58	0.26	0.0042	0.86	0.31	1.17
1391-G8.1	0.43	0.17	0.0030	0.78	0.42	1.20
1391-G9.1	0.60	0.32	0.0039	1.14	0.16	1.31
1391-G10.1	0.52	0.23	0.0037	0.85	0.33	1.18
Average				*0.86*	*0.32*	*1.18*
% S.D.				*12.17*	*21.42*	*4.32*
1394-R2A groundmass						
1391-G1.1	0.66	0.37	0.0035	1.46	0.12	1.58
1391-G2.1	0.53	0.32	0.0032	1.38	0.01	1.39
1391-G3.1	0.49	0.25	0.0032	1.08	0.20	1.27
1391-G4.1	0.78	0.48	0.0040	1.64	0.00	1.63
1391-G5.1	0.71	0.41	0.0044	1.29	0.06	1.35
1391-G6.1	0.50	0.28	0.0032	1.20	0.11	1.31
1391-G7.1	0.59	0.32	0.0034	1.28	0.16	1.44
1391-G8.1	0.38	0.24	0.0025	1.28	0.00	1.28
1391-G9.1	0.50	0.35	0.0030	1.40	0.00	1.40
Average				*1.33*	*0.07*	*1.41*
% S.D.				*12.08*	*105.82*	*9.03*
Torishima-48 groundmass						
48-G1.1	0.07		0.0025			0.24
48-G2.1	0.07		0.0026			0.22
48-G3.1	0.07		0.0023			0.27
48-G4.1	0.07		0.0023			0.25
48GM6	0.07		0.0026			0.23
48GM7	0.07		0.0026			0.22
48GM8	0.05		0.0027			0.16
48GM9	0.05		0.0027			0.17
48GM10	0.07		0.0027			0.22
48GM11	0.05		0.0023			0.19
48GM12	0.08		0.0023			0.28
Average						*0.22*
% S.D.						*17.31*
Torishima-48 inclusions						
48-PI1.1	0.07		0.0023			0.2638
48-PI2,1	0.06		0.0024			0.2227
48-PI3.1	0.06		0.0023			0.2380
48-PI4.1	0.13		0.0022			0.5228
Average						*0.31*
% S.D.						*45.43*

Density calculations were: Sumisu glasses=2400 g/l, Torishima groundmass=2373 g/l, Torishima inclusions=2300 g/l.

3.4. Sample thickness measurements from reflection spectra

Interference fringes form on reflection spectra of samples that have parallel surfaces, such as the doubly polished wafers studied here. Nishikida et al. (1996) noted, from a study of a thin silica film (3.5 μm) on a thick silica wafer, that the wavelength of the interference fringe pattern is directly proportional to the thickness and refractive index of the sample. Thus, thickness corresponds to the number of waves over any wavenumber interval, in the relationship:

$$\partial = m/2n(\nu 1 - \nu 2)$$

where m is the number of waves in a selected wavenumber range, n = refractive index of the sample, and $\nu 1$ and $\nu 2$ are the highest and lowest wavenumbers over the selected interval. The wavelength of the interference pattern does, however, increase at higher wavenumbers, but measurements made near $\nu = 2000$ cm^{-1} were found to be within error of the micrometer measurements (Fig. 2A).

There are several advantages to using reflection spectra to determine thickness measurements over micrometer measurements. First, the method is non-destructive whereas micrometer needles may break or crush the sample. Second, precision is high, as thickness is dependant on the wavenumber position, which is known to $<<1\%$, compared to substantial errors on thin samples measured by micrometer (e.g. a 2 μm uncertainty on the approximately 25 μm TS27-48 wafer results in an 8% error!). Third, reflection spectra measurements can be made immediately prior to, or after, transmission measurements used for analyte concentration determination. This allows the exact analytical area to be analysed, whereas micrometer nibs are difficult to place accurately, particularly on wafers with non-uniform thickness.

3.5. Errors for micro-FTIR and imaging-FTIR analysis

The error on analyte concentrations determined by micro- and imaging-FTIR analysis includes errors propagated from all variables of the Beer–Lambert law. For total water content, this was estimated at ± 10%, which is similar to previous studies (e.g. Dixon et al., 1988; Dixon et al., 1995; Macpherson et al., 1999; Agrinier and Jendrzejewski, 2000; Danyushevsky et al., 2000; Wysoczanski et al., 2006). For molecular water contents, the error may be significantly higher as some measured peak heights were small (only just detectable), and the position of the baseline for the 1630 cm^{-1} band (Fig. 2) is poorly constrained (King et al., 2002).

4. Results

Water species concentrations were measured by micro-FTIR in the centre of small (10–30 μm) patches of glass in the groundmass (Table 1). With the exception of 4 plagioclase-hosted melt inclusions in TS27-48, melt inclusions could not be analysed by micro-FTIR due to their small size. Groundmass glasses and melt inclusions were also analysed by imaging-FTIR to produce 24 spectrographic images, constructed from absorbance bands of total and molecular water (e.g. Fig. 3), and to determine water concentrations (Table 2). As absorbance is proportionally dependant to molar absorptivity, thickness and concentration, the intensity of the images reflects a combination of these variables. For homogenous substances of similar thickness, such as rhyolitic glasses analysed here, absorbance intensity will directly reflect differences in analyte concentration.

For the TS27-48 images, which contain large areas of groundmass glass, peak heights of the total water band were extracted from all 4096 spectra of the image, and subjected to a Chi-square test to determine the mean peak height of the total water band. Extracting peak heights for all spectra at any given absorbance band can be performed quickly and efficiently utilising spectra-manipulation software. The use of a Chi-square statistical test to determine mean values of a large data set is routinely used in Ion Microprobe dating of zircon (e.g. Sircombe, 2004; Wysoczanski and Allibone, 2004), and provides a weighted mean of the data at a 95% confidence level. This method utilises all of the data acquired in an image, as opposed to simply selecting an individual spectrum from an image that is considered to be representative of a sample.

4.1. Imaging-FTIR qualitative analysis

Qualitative analysis of images of total water peaks reveals a wide distribution of water throughout the samples. Patches of pure groundmass glass (e.g. Fig. 3A) show small changes in intensity that may indicate heterogeneity in water content. In TS27-48 images, groundmass glass occurs in large light- and dark-coloured patches and bands (Fig. 3C photomicrograph). These bands are also evident in spectroscopic images, with light- and dark-patches corresponding to areas of higher- and lower-intensity water peaks, respectively (Fig. 3C).

Many cracks can be seen in images from the groundmass to the interior of plagioclase phenocrysts. The majority are water-free, suggesting that they opened after crystallization, most likely during sample preparation. However, some cracks, particularly large non-linear

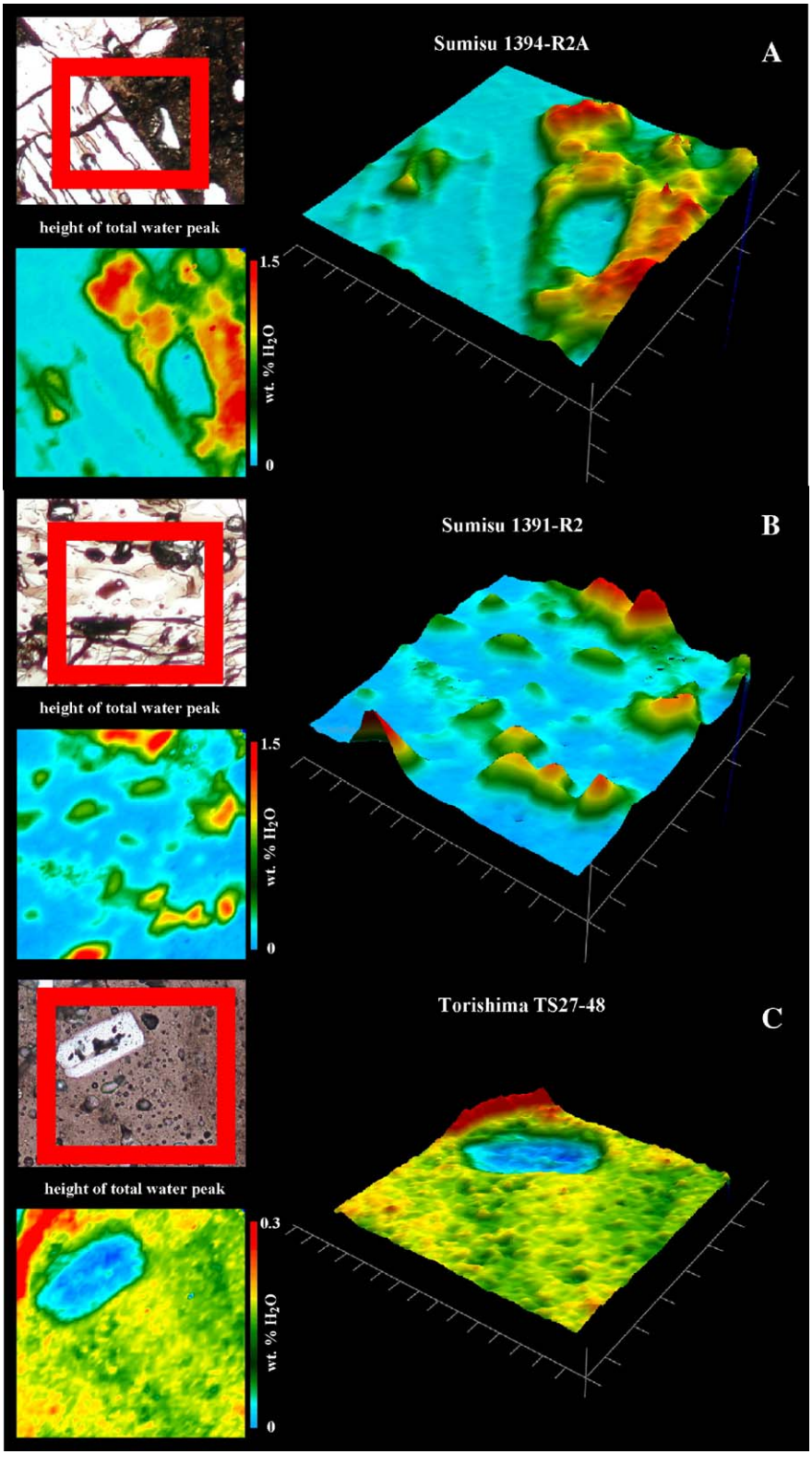
Sumisu 1394-R2A
A
height of total water peak
1.5
wt. % H2O
0
Sumisu 1391-R2
B
height of total water peak
1.5
wt. % H2O
0
Torishima TS27-48
C
height of total water peak
0.3
wt. % H2O
0

cracks, do contain traces of water (Fig. 3A). Water-bearing fractures also occur parallel and perpendicular to plagioclase cleavage planes. These connect long elongate melt inclusions, resulting in an open system network of inclusions and fractures, which in some cases intersect fractures extending from the groundmass to the edge of the phenocryst (Fig. 3A). By contrast, many smaller, spherical melt inclusions in resorbed honeycomb plagioclase do not have any apparent connection to other inclusions or to the groundmass (Fig. 3B). Many melt inclusions also contain vapour bubbles, formed from re-equilibration of the melt to lower pressures on the ascent of the magma. The presence of bubbles in the inclusions suggests that the inclusions remained closed since bubble formation, as the bubbles would have escaped open inclusions. FTIR imaging and analysis of individual spectra from the bubbles indicate that water contents of the bubbles are not noticeably different to areas of pure glass.

4.2. Water species concentrations and comparison between imaging-FTIR and micro-FTIR analysis

Total water contents of Sumisu groundmass glasses, determined by imaging-FTIR, range from 1.12–1.33 wt.% H_2O_{tot} (average 1.24 wt.%) in sample 1391-R2, and 1.25–1.61 wt.% H_2O_{tot} (average 1.44 wt.%) in sample 1394-R2A (Table 2, Fig. 4). Total water contents of TS27-48 groundmass glasses range from 0.17–0.26 wt.% H_2O_{tot} (average 0.20 wt.%). Water contents determined by micro-FTIR average 1.18, 1.41 and 0.22 wt.% H_2O_{tot} for samples 1391-R2, 1394-R2A and TS27-48, respectively (Table 1). These values are within analytical uncertainty of the imaging-FTIR analyses (Fig. 4).

Sumisu groundmass glasses have total water contents higher than expected for melts solidifying at magmatic temperatures (900–1000 °C; Shukuno et al., 2006-this issue) and their pressure of eruption (Fig. 5). However, the solubility of water in silicic melts is inversely proportional to temperature (Yamashita, 1999), and water contents of the glasses are consistent with temperatures of 700–800 °C for sample 1391-R2, and 600–700 °C for 1394-R2A (with two exceptions at 500–550 °C) at their eruption pressure, using current water solubility models (Newman and Lowenstern, 2002) (Fig. 5). The low total water contents measured in TS27-48 groundmass glasses are consistent with eruption at or near atmospheric pressure (Newman and Lowenstern, 2002).

Molecular water is the dominant water species in Sumisu groundmass glasses (Tables 1 and 2). Imaging-FTIR and micro-FTIR analyses indicate approx. 65–75% of water in sample 1391-R2 is H_2O_{mol}. The proportion of water species in sample 1394-R2A differs between the techniques, with imaging-FTIR indicating an average of 74% of water is H_2O_{mol}, whereas micro-FTIR indicates that nearly all water is H_2O_{mol}. The discrepancy may be due to the large errors associated with measuring the 1630 cm^{-1} band. Despite the large analytical uncertainty, the ratio of H_2O_{mol} to OH^- is significantly higher than predicted by speciation models for rhyolitic melts at magmatic temperatures (approximately 20% of H_2O_{mol}; Newman and Lowenstern, 2002). High proportions of H_2O_{mol} are consistent with slow cooling, which drives the water solubility reaction ($H_2O_{mol}+O=> 2OH^-$) to the left, resulting in a substantially higher H_2O_{mol}:OH^- ratio (Zhang et al., 1997). Rhyolitic magmas cooling rates have been documented to be as slow as 0.001 K/min, allowing water contents to equilibrate to the glass transition temperature (Gottsmann and Dingwell, 2002), estimated at 600–800 °C for the Sumisu groundmass glasses (Fig. 5).Water speciation could not be determined for sample TS27-48 due to low water contents resulting in low detection limits for molecular water.

Imaging-FTIR analyses of melt inclusions indicate similar average total water contents of 1.18 wt.% H_2O_{tot} in 1391-R2 and 1.24 wt.% H_2O_{tot} in 1394-R2A, with a total range of 1.02–1.38 wt.% H_2O_{tot}. This is within error of the Sumisu 1391-R2 groundmass glasses, but lower than Sumisu 1394-R2A groundmass glasses. The proportion of water species in inclusions is indistinguishable to that of the groundmass glasses, with high molecular water contents suggesting slow cooling.

Melt inclusions in plagioclase from TS27-48 have a wide range in total water content (0.22–0.41 wt.% H_2O_{tot}) that is significantly higher than groundmass glass water contents (0.18–0.26 wt.% H_2O_{tot}). Four melt

Fig. 3. Representative spectroscopic images of the total water absorbance height (ν=3550 cm^{-1}) from Sumisu and Torishima samples. Colour intensity and height in 3-D images reflects the height of the water peak and not water content, as peak height is dependant on water content, thickness of sample and molar absorptivity. Photomicrographs at top left of each image show the area analysed. Scale is 350 μm across each image. Isolated pixels of high intensity resulting from saturated signals in individual FPA channels occur. (A) Sample Sumisu 1394-R2A, showing small (<20 μm) patches of glass in microcrystalline groundmass and a large plagioclase phenocryst with elongate melt inclusions and parallel and orthogonal fractures. (B) Resorbed honeycomb plagioclase phenocryst from sample Sumisu 1391-R2, with multiple melt inclusions, some of which are open system (connected) and others appear closed (isolated inclusions). (C) Torishima-48 sample glass with small plagioclase phenocryst. Note the water-rich band at top left, which is residual epoxy not dissolved from a fracture of the sample wafer during sample processing. Glass occurs as patches with slightly higher (light coloured glass in photomicrograph) and lower water contents (dark coloured glass).

Table 2
Imaging FTIR analysis

Analysis	Abs (3550 cm^{-1})	Abs (1630 cm^{-1})	Thickness (cm)	H_2O_{mol} wt.%	OH^- wt.%	H_2O_{total} wt.%
1391-R2 groundmass						
1	0.77	0.34	0.0050	0.94	0.36	1.30
2	0.68	0.27	0.0050	0.73	0.42	1.15
3	0.62	0.33	0.0040	1.13	0.18	1.31
4	0.53	0.24	0.0040	0.81	0.31	1.12
5	0.63	0.31	0.0040	1.07	0.26	1.33
6	0.58	0.22	0.0040	0.76	0.46	1.22
7	0.62	0.29	0.0040	1.00	0.30	1.30
8	0.59	0.20	0.0043	0.65	0.50	1.15
9	0.67	0.24	0.0043	0.77	0.54	1.30
10	0.62	0.18	0.0040	0.63	0.68	1.31
11	0.57	0.22	0.0040	0.77	0.42	1.19
12	0.63	0.23	0.0040	0.78	0.54	1.32
13	0.55	0.18	0.0040	0.63	0.53	1.16
14	0.29	0.09	0.0019	0.65	0.63	1.29
15	0.27	0.09	0.0019	0.67	0.54	1.21
16	0.26	0.11	0.0019	0.81	0.34	1.16
Average				0.80	0.44	1.24
% S.D.				19.50	31.88	5.96
1391-R2 inclusions						
1	0.59	0.15	0.0040	0.51	0.71	1.22
2	0.20	0.09	0.0015	0.78	0.33	1.11
3	0.18	0.06	0.0015	0.55	0.46	1.02
4	0.32	0.15	0.0025	0.83	0.23	1.06
5	0.36	0.14	0.0025	0.77	0.42	1.19
6	0.51	0.22	0.0035	0.84	0.38	1.22
7	0.51	0.27	0.0035	1.04	0.18	1.22
8	0.19	0.08	0.0015	0.75	0.30	1.05
9	0.33	0.11	0.0020	0.75	0.63	1.38
10	0.33	0.11	0.0020	0.77	0.59	1.36
11	0.14	0.05	0.0010	0.64	0.49	1.13
Average				0.75	0.43	1.18
% S.D.				19.25	38.92	10.17

Analysis	Abs (3550 cm^{-1})	Abs (1615 cm^{-1})	Thickness (cm)	H_2O_{mol} wt.%	OH^- wt.%	H_2O_{total} wt.%
1394-R2A groundmass						
1	0.68	0.30	0.0040	1.02	0.39	1.42
2	0.61	0.26	0.0040	0.90	0.37	1.27
3	0.70	0.33	0.0040	1.14	0.33	1.47
4	0.67	0.29	0.0040	0.97	0.43	1.41
5	0.73	0.36	0.0040	1.24	0.29	1.53
6	0.73	0.36	0.0040	1.22	0.31	1.53
7	0.63	0.32	0.0040	1.08	0.23	1.31
8	0.62	0.33	0.0035	1.28	0.18	1.47
9	0.57	0.29	0.0035	1.13	0.24	1.37
10	0.84	0.30	0.0047	0.87	0.62	1.48
11	0.70	0.30	0.0047	0.87	0.38	1.25
12	0.86	0.38	0.0047	1.12	0.42	1.53
13	0.64	0.23	0.0037	0.83	0.61	1.44
14	0.67	0.29	0.0037	1.06	0.45	1.51
15	0.69	0.30	0.0037	1.12	0.44	1.55
16	0.65	0.30	0.0040	1.01	0.34	1.35
17	0.68	0.33	0.0040	1.11	0.30	1.41
18	0.77	0.36	0.0040	1.23	0.38	1.61
19	0.71	0.31	0.0040	1.06	0.43	1.49
Average				1.07	0.37	1.44
% S.D.				12.47	30.11	6.80
1394-R2A inclusions						
1	0.22	0.12	0.0015	1.09	0.10	1.19
2	0.11	0.05	0.0008	0.92	0.31	1.23
3	0.09	0.04	0.0007	0.82	0.35	1.17
4	0.49	0.22	0.0035	0.85	0.32	1.17
5	0.56	0.27	0.0035	1.04	0.29	1.33
6	0.42	0.15	0.0030	0.67	0.48	1.15
7	0.42	0.21	0.0025	1.13	0.27	1.41
8	0.47	0.19	0.0030	0.84	0.47	1.31
9	0.52	0.28	0.0032	1.18	0.17	1.35
10	0.28	0.17	0.0020	1.16	0.00	1.16
11	0.44	0.23	0.0032	0.96	0.20	1.15
Average				0.97	0.27	1.24
% S.D.				16.87	53.70	7.52

Analysis	Abs (3550 cm^{-1})	Thickness (cm)	H_2O_{total} wt.%
TS27-48 inclusions			
1	0.03	0.0010	0.22
2	0.08	0.0025	0.26
3	0.12	0.0025	0.41
4	0.05	0.0015	0.28
5	0.06	0.0015	0.37
6	0.04	0.0010	0.32
7	0.04	0.0010	0.36
Average			0.32
% S.D.			21.10
TS27-48 groundmass			
1	0.05	0.0023	0.17
2	0.05	0.0023	0.18
3	0.07	0.0025	0.23
4	0.07	0.0026	0.24
5	0.06	0.0026	0.20
6	0.07	0.0022	0.26
7	0.05	0.0020	0.19
8	0.05	0.0020	0.21
9	0.05	0.0021	0.22
10	0.05	0.0021	0.19
11	0.05	0.0021	0.21
12	0.05	0.0021	0.19
13	0.05	0.0021	0.18
Average			0.20
% S.D.			12.53
TS27-48 average groundmass			
1 (n = 2239)	0.05	0.0022	0.18
2 (n = 647)	0.07	0.0025	0.22
3 (n = 979)	0.07	0.0026	0.23
4 (n = 702)	0.05	0.0021	0.19
5 (n = 1341)	0.05	0.0020	0.19
6 (n = 696)	0.05	0.0021	0.21
7 (n = 2726)	0.05	0.0021	0.20
Average			0.20
% S.D.			8.97

TS27–48 average groundmass concentrations were determined using Chi–square test on all glass spectra (n) from an image. See text for discussion. Density calculations were: Sumisu and inclusions = 2400 g/l, Torishima inclusions = 2300 g/l.

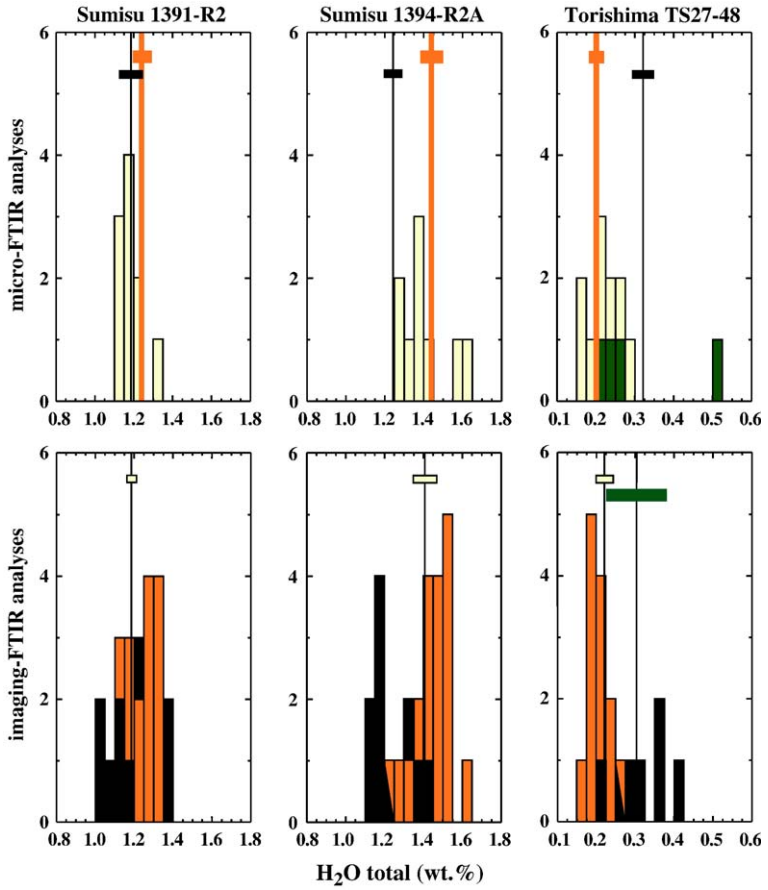

Fig. 4. Water contents of Izu–Bonin groundmass glasses and melt inclusions in resorbed honeycomb plagioclase phenocrysts measured by micro-FTIR and imaging-FTIR. Thin lines correspond to average water contents of each sample determined by the alternate technique (micro- or imaging-FTIR) to that shown for histograms in that plot. Error bars of average values are percent standard deviation. Torishima Volcano groundmass glasses measured by imaging-FTIR were calculated from average representative spectra, and from weighted means of all spectra in an image.

inclusions were large enough to be analysed by micro-FTIR using the 20 μm aperture. Three have 0.22–0.26 wt.% H_2O_{tot}, comparable to the groundmass glasses, but a fourth has a higher H_2O_{tot} content of 0.52 wt.%.

5. Discussion

5.1. Significance of melt inclusion water contents

Spectroscopic imaging and optical examination of melt inclusions in honeycomb plagioclase from Sumisu Caldera and Torishima Volcano reveal that open cracks connect some of the inclusions to the surface of the host mineral. The similar water content of these inclusions to groundmass glasses suggests that they degassed water as they equilibrated to pressures and temperatures of eruption. Other inclusions, however, are not connected to the surface but appear to be fully trapped within the host mineral (Fig. 3).

Melt inclusions that have remained enclosed in a phenocryst can provide a direct measurement of the water content of the magma at the time of entrapment, as they are not susceptible to degassing at eruption pressures. For example, inclusions in honeycomb plagioclase from the Kermadec arc, offshore New Zealand, have 2.3 wt.% H_2O_{tot}, substantially higher than the groundmass glasses that have degassed to eruption pressures, and contain just 0.17 wt.% H_2O_{tot} (Wysoczanski et al., 2006). Similarly, the higher water contents of melt inclusions with higher water contents than groundmass glasses in TS27-48 may not have degassed, or have only partially degassed. Water concentrations of closed inclusions, however, may change due to crystallisation of minerals inside or onto the wall of the inclusion, or from diffusion of hydrogen between the inclusion and host magma (Danyushevsky et al., 2002).

Inclusions analysed here are free of microphenocrysts, and crystallisation of minerals onto the wall of

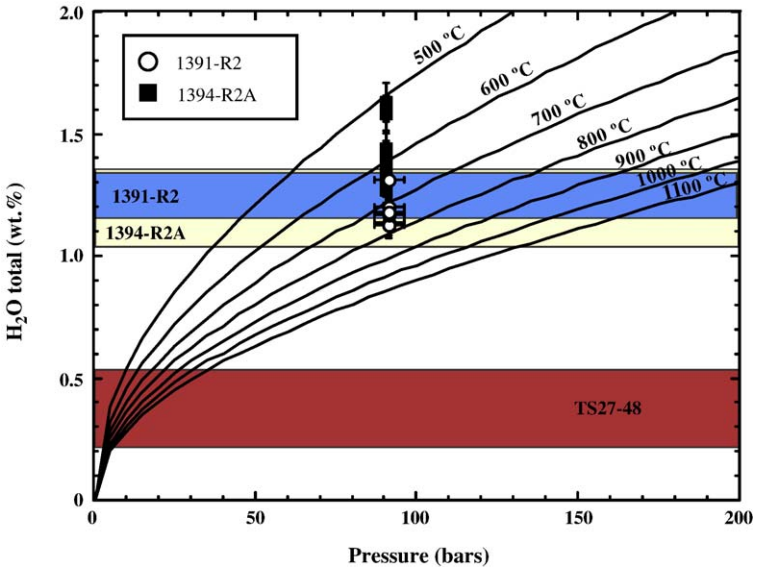

Fig. 5. Water solubility plot (Newman and Lowenstern, 2002) of felsic glasses at variable temperature and pressure. Groundmass glass compositions of Sumisu Caldera samples are plotted as points against the pressure of their depth of collection. Total water contents of inclusions from all samples are shown as horizontal fields, as their pressure of entrapment is uncertain.

the phenocryst is not visible. Diffusion of hydrogen is more difficult to determine. The slow cooling of the inclusions may have resulted in lower hydrogen fugacity in the inclusions relative to the host magma, resulting in diffusion of hydrogen into the inclusion. Conversely, loss of hydrogen from the inclusion may also have occurred, although the absence of magnetite dust in the inclusions suggests that any hydrogen loss was minimal (Danyushevsky et al., 2002).

Despite evidence that these inclusions have remained closed, their similar water contents to both open inclusions and groundmass glasses suggests that they have also equilibrated to eruption pressures, through diffusion or degassing of water. One simple test to determine if they have lost water species would be to analyse samples collected at greater water depths. If the inclusions in those samples have degassed, then their water contents will have equilibrated to eruptive temperatures and pressures. However, if their water contents are similar to that of closed inclusions analysed here, then it is likely that they have not degassed with eruption onto the seafloor.

5.2. Possible implications for models of silicic crustal growth

Honeycomb plagioclase in arc magmas can form as a skeletal texture with rapid growth during supercooling, or due to partial dissolution of plagioclase when it is in disequilibrium with the host magma (Kawamoto, 1992). The rhyolitic composition of the Izu–Bonin melt inclusions in honeycomb plagioclase with high-An cores (Shukuno et al., 2006-this issue) suggests that they formed by partial dissolution of plagioclase that had initially crystallised from a mafic magma. This is consistent with models of partial melting of andesitic or basaltic crust producing a rhyolitic magma (Tamura and Tatsumi, 2002; Shukuno et al., 2006-this issue), or of plagioclase derived from basaltic or andesitic magmas being entrained in younger silicic magmas of uncertain origin. The water contents of the melt inclusions at the time of entrapment will reflect the composition of the source of the silicic magmas.

The pre-eruptive water contents of the silicic magmas can only be inferred to have been equal to or greater than concentrations measured in the inclusions and groundmass glasses, as it is likely that they have lost water by degassing and/or diffusion. However, the anhydrous mineral assemblage of all silicic lavas from the Izu–Bonin arc suggests a relatively dry source. This is more consistent with partial melting of a dry or damp crust, than with partial melting of water-rich crust or differentiation of basaltic magma, as the silicic products of these processes would have high water contents, and crystallise hydrous minerals as they evolve. Further analysis of melt inclusions in silicic rocks from the Izu–Bonin arc, particularly those collected at greater depths, will help further elucidate the pre-eruptive water content of the magmas, and the composition of their source.

5.3. Application of imaging to studies of volcanic materials

In addition to the application shown here, spectroscopic imaging has the potential for investigating many other volcanic processes and products. For example, experiments to examine diffusion, particularly in homogenising melt inclusions using heating stages (Danyushevsky et al., 2002) are an ideal application of the technique as imaging can capture near-instantaneous time-series images of the homogenisation process, in addition to providing both qualitative and quantitative data. Another similar application would be tracing the flow of fluids in serpentinites and eclogites from the descending slab, which is an important process in refertilisation of the mantle, partial melting and subsequent growth of silicic crust (e.g. Tatsumi and Eggins, 1995; Hattori and Guillot, 2003; Wysoczanski et al., 2006). Imaging-FTIR can also be used to determine modal populations of groundmass phases (Fig. 3) from statistical treatment of imaging spectra. For example, the proportion of groundmass glass can be estimated from the proportion of spectra with characteristics of glass. Hydrous and anhydrous mineral phases can be estimated from remaining spectra that contain or do not contain water, respectively. Vesicle content can also be determined, simply from the number of spectra that do not have silica absorbance bands.

6. Conclusions

Spectroscopic FTIR-imaging, applied to silicic volcanic glasses from the Izu–Bonin arc, provides comparable water species concentration measurements to conventional micro-FTIR analysis, at a similar precision. In addition, it has the advantage of higher spatial resolution (5 μm) allowing small-scale heterogeneities in water content to be distinguished and inclusions that are too small for micro-FTIR analysis to be analysed. Furthermore, it can provide a visual image of the distribution of water species in the sample. Reflection spectra, obtained by either imaging- or micro-FTIR analysis can provide high-precision thickness measurements of a sample, and is a reliable alternative to micrometer measurements, especially for thin samples (<50 μm) where using a micrometer may impart significant error on analyses, and damage the sample.

Groundmass glasses in silicic lavas from Sumisu Caldera and Torishima Volcano contain water contents consistent with equilibration to their pressures of eruption. Water contents of melt inclusions in Sumisu Caldera plagioclase have similar water contents to the groundmasses glasses (<1.5 wt.% H_2O_{tot}), suggesting that they may also have lost water through degassing and/or diffusion. Torishima Volcano melt inclusions have water contents (up to 0.5 wt.% H_2O_{tot}) that are higher than groundmass glasses (0.2 wt.% H_2O_{tot}). Degassing and/or diffusion of water from these inclusions cannot be discounted. Although the pre-eruptive water content of the silicic magmas could not be determined from this study, the anhydrous mineral assemblage of all silicic lavas from the Izu–Bonin arc suggests a source with low water content, consistent with partial melting models of dry, or damp, mid-lower crust.

Acknowledgements

We thank the captain and the crew of the research vessel R.V. *Natsushima* and the manned submersible *Shinkai2000,* from which the samples were collected from Sumsiu Caldera. We also thank A.R.L Nichols and S. Yamashita for their helpful and constructive reviews, and H. Shukuno, Y. Tamura and Y. Tatsumi for the access to the data and/or discussions.

References

Agrinier, P., Jendrzejewski, N., 2000. Overcoming problems of density and thickness measurements in FTIR volatile determinations: a spectroscopic approach. Contrib. Mineral. Petrol. 139, 265–272.

Aramaki, S., Ui, T., 1978. Major element frequency distribution of the Japanese Quaternary volcanic rocks. Bull. Volcanol. 41, 390–407.

Danyushevsky, L.V., Eggins, S.M., Falloon, T.M., Christie, D.M., 2000. H_2O abundance in depleted to moderately enriched mid-ocean ridge magmas; Part I: incompatible behaviour, implications for mantle storage, and origin of regional variations. J. Petrol. 41, 1329–1364.

Danyushevsky, L.V., McNeill, A.W., Sobolev, A.V., 2002. Experimental and petrological studies of melt inclusions in phenocrysts from mantle-derived magmas: an overview of techniques, advantages and complications. Chem. Geol. 183, 5–24.

Dixon, J.E., Clauge, D.A., 2001. Volatiles in basaltic glasses from Loihi Seamount, Hawaii. J. Petrol. 42, 627–654.

Dixon, J.E., Stolper, E.M., Delaney, J.R., 1988. Infrared spectroscopic measurements of CO_2 and H_2O glasses in the Juan de Fuca Ridge basaltic glasses. Earth Planet. Sci. Lett. 90, 87–104.

Dixon, J.E., Stolper, E.M., Holloway, J.R., 1995. An experimental study of water and carbon dioxide solubilities in mid-ocean ridge basaltic liquids. Part I: calibration and solubility models. J. Petrol. 36, 1607–1631.

Dixon, J.E., Leist, L., Langmuir, C.H., Schilling, J.-G., 2002. Recycled dehydrated lithosphere observed in plume-influenced mid-ocean-ridge basalt. Nature 420, 385–398.

Dobson, P.F., Epstein, S., Stolper, E.M., 1989. Hydrogen isotope fractionation between coexisting vapor and silicate glasses and melts at low pressure. Geochim. Cosmochim. Acta 53, 2723–2730.

Fiske, R.S., Naka, J., Iizasa, K., Yuasa, M., Klaus, A., 2001. Submarine silicic caldera at the front of the Izu–Bonin arc, Japan: voluminous

seafloor eruptions of rhyolite pumice. Geol. Soc. Am. Bull. 113, 813–824.

Gottsmann, J., Dingwell, D.B., 2002. The thermal history of a splatter-fed lava flow: the 8-ka pantellerite flow of Mayor Island, New Zealand. Bull. Volcanol. 64, 410–422.

Hattori, K.H., Guillot, S., 2003. Volcanic fronts form as a consequence of serpentinite dehydration in the forearc mantle wedge. Geology 31, 525–528.

Hauri, E., Wang, J., Dixon, J.E., King, P.L., Mandeville, C., Newman, S., 2002. SIMS analyses of volatiles in volcanic glasses. 1: calibration, matrix effects and comparisons with FTIR. Chem. Geol. 183, 99–114.

Ihinger, P.D., Hervig, R.L., McMillan, P.F., 1994. Applications of experimental results to C–O–H species in natural melts. Mineral. Soc. Am. Rev. Min. 30, 67–121.

Ito, Y., Nakashima, S., 2002. Water distribution in low-grade siliceous metamorphic rocks by micro-FTIR and its relation to grain size: a case from the Kanto Mountain region, Japan. Chem. Geol. 189, 1–18.

Kawamoto, T., 1992. Dusty and honeycomb plagioclase: indicators of processes in the Uchino stratified magma chamber, Izu Peninsula, Japan. J. Volcanol. Geotherm. Res. 49, 191–208.

Kawate, S., Arima, M., 1998. Petrogenesis of the Tanzawa plutonic complex, central Japan: exposed felsic middle crust of the Izu–Bonin–Mariana arc. Isl. Arc 7, 342–358.

King, P.L., Vennemann, T.W., Holloway, J.R., Hervig, R.L., Lowenstern, J.B., Forneris, J.F., 2002. Analytical techniques for volatiles: a case study using intermediate (andesitic) glasses. Am. Mineral. 87, 1077–1089.

Lewis, E.N., Treado, P.J., Reeder, R.C., Story, G.M., Dowrey, A.E., Marcott, C., Levin, I.W., 1995. Fourier Transform Spectroscopic Imaging using an Infrared Focal-Plane Array Detector. Anal. Chem. 67 (19), 3377–3381.

Luhr, J.F., 2001. Glass inclusions and melt volatile contents at Parícutin Volcano, México. Contrib. Mineral. Petrol. 142, 261–283.

Macpherson, C.G., Hilton, D.R., Newman, S., Mattey, D.P., 1999. CO_2, $^{13}C/^{12}C$ and H_2O variability in natural basaltic glasses: a study comparing stepped heating and FTIR spectroscopic techniques. Geochim. Cosmochim. Acta 63, 1805–1813.

Nagaoka, D., Okino, K., Kato, S., 1991. Landforms of submarine volcanoes in central part of the Izu–Ogasawara arc, by multi-beam sounding system. Rep. Hydrogr. Res. 27, 145–172.

Nakajima, K., Arima, M., 1998. Melting experiments on hydrous low-K tholeiite: implications for the genesis of tonalitic crust in the Izu–Bonin–Mariana arc. Isl. Arc 7, 359–373.

Nakamoto, K., 1978. Infrared and Raman Spectra of Inorganic and Coordination Compounds. John Wiley, New York. 448p.

Newman, S., Lowenstern, J.B., 2002. VolatileCalc: a silicate melt-H_2O–CO_2 solution model written in Visual Basic for Excel. Comput. Geosci. 28, 597–604.

Newman, S., Stolper, E.M., Epstein, S., 1986. Measurement of water in rhyolitic glasses-calibration of an infrared spectroscopic technique. Am. Mineral. 71, 1527–1541.

Newman, S., Stolper, E., Stern, R., 2000. H_2O and CO_2 in magmas from the Mariana arc and back arc system. Geochem. Geophys. Geosys. 1 (5). doi:10.1029/1999GC000027.

Nichols, A.R.L., Carroll, M.R., Hoskuldsson, A., 2002. Is the Iceland hot spot also wet? Evidence from the water contents of undegassed submarine and subglacial pillow basalts. Earth Planet. Sci. Lett. 202, 77–87.

Nishikida, K., Nishio, E., Hannah, R.W., 1996. Selected Applications of Modern FT-IR Techniques. Gordon and Breach. 200 pp.

Shukuno, H., Tamura, Y., Tani, K., Chang, Q., Suzuki, T., Fiske, R.S., 2006. Origin of silicic magmas and the compositional gap at Sumisu submarine caldera, Izu–Bonin arc, Japan. J. Volcanol. Geotherm. Res. 156, 187–216. doi:10.1016/j.jvolgeores.2006.03.018.

Signorelli, S., Vaggelli, G., Romano, C., 1999. Pre-eruptive volatile (H_2O, F, Cl, S) contents of phonolitic magmas feeding the 3550-year old Avellino eruption from Vesuvius, southern Italy. J. Volcanol. Geotherm. Res. 93, 237–256.

Sircombe, K.N., 2004. AgeDisplay; an EXCEL workbook to evaluate and display univariate geochronological data using binned frequency histograms and probability density distributions. Comput. Geosci. 30, 21–31.

Sobolov, A.V., Chaussidon, M., 1996. H_2O concentrations in primary melts from supra-subduction zones and mid-ocean ridges: implications for H_2O storage and recycling in the mantle. Earth Planet. Sci. Lett. 137, 45–55.

Takahashi, N., Suyehiro, K., Shinohara, M., 1998. Implications from the seismic crustal structure of the northern Izu–Bonin arc. Isl. Arc 7, 383–394.

Tamura, Y., Tatsumi, Y., 2002. Remelting of an andesitic crust as a possible origin for rhyolitic magma in oceanic arcs; an example from the Izu–Bonin arc. J. Petrol. 43 (6), 1029–1047.

Tatsumi, Y., Eggins, S.M., 1995. Subduction Zone Magmatism. Blackwell, Cambridge. 211p.

Vogel, T.A., Patino, L.C., Alvarado, G.E., Gans, P.B., 2004. Silicic ignimbrites within the Costa Rican volcanic front: evidence for the formation of continental crust. Earth Planet. Sci. Lett. 226, 149–159.

Wysoczanski, R.J., Allibone, A.H., 2004. Age, correlation and provenance of the Neoproterozoic Skelton Group, Antarctica: Grenville age detritus on the margin of East Antarctica. J. Geol. 112, 401–416.

Wysoczanski, R.J., Wright, I.C., Gamble, J.A., Hauri, E.H., Luhr, J.F., Eggins, S.M., Handler, M.R., 2006. Volatile contents of Kermadec Arc–Havre Trough pillow glasses; fingerprinting slab-derived aqueous fluids in the mantle sources of arc and back-arc lavas. J. Volc. Geotherm. Res. 152, 51–73.

Yamashita, S., 1999. Experimental study of the effect of temperature on water solubility in natural rhyolite melt to 100 MPa. J. Petrol. 40 (10), 1497–1507.

Yuasa, M., Murakami, F., Sato, E., Watanabe, K., 1991. Submarine topography of seamounts on the volcanic front of the Izu–Ogasawara (Bonin) arc. Bull. Geol. Surv. Japan 42, 703–743.

Zhang, Y., Jenkins, J., Zhengjui, X., 1997. Kinetics of the reaction $H_2O + O \Leftrightarrow 2OH$ in rhyolitic glasses upon cooling: geospeedometry and comparison with glass transition. Geochim. Cosmochim. Acta 61, 11, 2167–2173.